

# Methodology of elastic full-waveform inversion of multicomponent ocean-bottom data for anisotropic media

Harpreet Sethi<sup>1,2</sup>  | Ilya Tsvankin<sup>2</sup> | Jeff Shragge<sup>2</sup>

<sup>1</sup>NVIDIA Corporation, Santa Clara, California, USA

<sup>2</sup>Department of Geophysics, Colorado School of Mines, Golden, Colorado, USA

## Correspondence

Harpreet Sethi, Colorado School of Mines, Department of Geophysics, 80401, Golden, Colorado, USA. Email: hsethi@mines.edu

## Funding information

Colorado School of Mines

## Abstract

Full-waveform inversion of multicomponent data can provide an improved estimation of medium parameters using both compressional- and shear-wave information. However, most earlier studies that involved a full-waveform inversion of ocean-bottom data are based on acoustic anisotropic or elastic isotropic approximations. Here, we consider realistic elastic anisotropic media and develop an efficient full-waveform inversion framework for estimating model parameters. We simulate seismic wavefields using a previously developed coupled acoustic/elastic wave propagator that implements a mimetic finite-difference method with fully staggered grids to accurately handle the fluid/solid boundary conditions. The algorithm employs a multiscale approach starting from low frequencies and incorporating higher frequency bands in the later inversion stages. We analyse the influence of different types of input data on the accuracy of the inverted anisotropy parameters for hard and soft water bottoms. The employed misfit function incorporates information from both hydrophones and ocean-bottom geophones. Numerical examples indicate that injecting multiple data components simultaneously increases the complexity of the objective function and often degrades the quality of the estimated medium parameters. Thus, we propose a sequential strategy using a single data component at a time. Pressure (hydrophone) data alone can provide satisfactory results if long offsets (i.e., with the offset/depth ratio  $\geq 3$ ) are available. Adding the horizontal particle-displacement or -velocity components increases the accuracy of the estimated shear-wave vertical velocity ( $V_{S0}$ ) and P-wave normal-moveout ( $V_{\text{nmo}, p}$ ) velocity, especially for strongly heterogeneous sub-water-bottom models.

## KEYWORDS

acoustics, elastics, anisotropy, full waveform, inversion, seismics, inverse problem

## INTRODUCTION

In marine seismic environments, the application of ocean-bottom acquisition systems (nodes or cables) is becoming increasingly popular because of their ability to record four-component (4-C) data (i.e., 3-C sensors recording particle velocity and a single hydrophone recording pressure). Multicomponent data provide information about the S-wave

velocity model and anisotropy parameters (Farfour and Yoon, 2016). Ocean-bottom acquisition systems (OBS) usually provide a wider azimuthal coverage and higher signal-to-noise ratio than streamer acquisition and acquire data that are less likely than streamer data to be contaminated by water waves and boat noise. Another advantage of OBS is its ability to record data continuously for long periods of time, which can be highly beneficial for time-lapse reservoir monitoring.

Elastic full-waveform inversion (EFWI) of multicomponent data can be used to evaluate the elastic subsurface properties and reservoir attributes. Unlike travelttime-based tomography methods (Zelt and Smith, 1992), EFWI uses both amplitude and phase information to invert for the medium parameters (Tarantola, 1986; Mora, 1987; Irnaka et al., 2022; Pladys et al., 2022; Chen et al., 2022). For example, Sears et al. (2008) use both particle-velocity and hydrophone data to estimate the P- and S-wave velocities in elastic isotropic media from ocean-bottom-cable (OBC) records. They show that the inversion of P-wave data using vertical particle velocity is more robust compared to that using hydrophone data. In the presence of a soft water bottom, converted PS-waves recorded on horizontal particle-velocity components are essential for obtaining high-resolution S-wave velocity models. Vigh et al. (2014) propose an objective function that combines pressure and particle velocity for estimating the P- and S-wave velocities. They employ a multiscale approach starting from low frequencies and emphasize the importance of judiciously weighting different data components. Sun and Jin (2020) also use a combined misfit function to incorporate both pressure and particle-velocity components for ocean-bottom nodes into full-waveform Inversion (FWI) for isotropic media. They employ a modified acoustic-elastic coupled equation for wavefield modelling, which allows them to directly simulate pressure. However, their methodology does not properly account for the fluid/solid boundary conditions at the seafloor.

Most earlier applications of FWI to anisotropic media are limited to acoustic approximations (Gholami et al., 2013; Plessix & Cao, 2011). Operto et al. (2015) apply frequency-domain FWI to invert for the P-wave vertical velocity ( $V_{P0}$ ) in viscoacoustic transversely isotropic media with a vertical symmetry axis (VTI). Kamath and Tsvankin (2016) and Kamath et al. (2017) conduct an FWI sensitivity analysis for multicomponent data from elastic VTI media with the goal of identifying an optimal parameterization. Guitton and Alkhalifah (2017) also perform a sensitivity analysis for elastic VTI media using FWI of near-seafloor pressure records. However, the sensitivity of FWI results to the composition of the input data (i.e., which components are included and in what combination or sequence) has rarely been studied for OBS surveys. In practice, the horizontal components (particle velocity or displacement) are rarely employed due to poor data quality and/or an incomplete understanding of the complex wave phenomena at the seafloor. In addition, most modelling codes approximately treat the water layer as a solid with vanishing S-wave velocity, which leads to incorrect acoustic-elastic boundary condition implementations at the seafloor.

Using a fluid/solid coupled wave propagator instead of a more conventional single-domain elastic propagator offers many advantages, especially for EFWI of offshore data. First, it is more computationally efficient to solve the acoustic rather than the elastic wave equation within the water layer. Second,

incorrect fluid/solid boundary condition implementations can distort the surface- and body-wave amplitudes (Sethi et al., 2021). Qu et al. (2020) use a coupled fluid/solid propagator in an EFWI scheme for estimating the parameters of isotropic media from OBC data. They employ the curvilinear coordinates-based finite-difference method with the correct fluid/solid boundary conditions at the seafloor. They also use mode separation to reduce the crosstalk between P- and S-wave velocities. Cao et al. (2022) implement the spectral-element method to devise a coupled fluid/solid propagator and perform FWI for isotropic media.

In this work we use our previously developed mimetic finite-difference method that accurately incorporates the correct fluid/solid boundary conditions (Sethi et al., 2021) as the modelling engine to perform anisotropic EFWI of both pressure records and particle-velocity components. A weighted data-difference objective function that combines pressure records and multicomponent seafloor data is minimized for estimating the parameters of two-dimensional VTI media. The paper begins with a review of wave propagation in the presence of a fluid/solid interface and of the boundary conditions in anisotropic media. We then discuss the formulation of the inverse problem and the weighted data-difference FWI objective function. The adjoint-state method is employed to derive the adjoint fluid/solid coupled system and the gradients of the objective function for arbitrarily anisotropic media. Several inversion strategies that combine different data components are tested on realistic synthetic models. We discuss the inversion results and identify practical approaches to EFWI of ocean-bottom data. Numerical experiments demonstrate that a sequential strategy using all data components performs best for different types of anisotropic underwater models.

## THEORY

The three-dimensional elastic wave equation for a heterogeneous elastic anisotropic medium can be written as

$$\rho^s \dot{\mathbf{v}}^s = \nabla \cdot \boldsymbol{\sigma} + \mathbf{b}^s, \quad (1)$$

where  $\rho^s$  is the density,  $\mathbf{v}^s$  is the particle velocity, the dot indicates a temporal derivative,  $\boldsymbol{\sigma}$  is the stress tensor,  $\nabla \cdot$  denotes the divergence operation,  $\mathbf{b}^s$  is the body force per unit volume and the superscript 's' indicates a material property or wavefield variable defined in the solid (elastic) domain. We also use the following linear constitutive relationship (generalized Hooke's law) to link the temporal derivatives of the stress ( $\sigma_{ij}$ ) and strain ( $\epsilon_{kl}$ ) tensors:

$$\dot{\boldsymbol{\sigma}} = \mathbf{C} : \dot{\boldsymbol{\epsilon}}, \quad (2)$$

where  $C$  is the stiffness tensor, ‘:’ denotes a double tensor contraction operation and the temporal derivative of the strain tensor is given by

$$\dot{\epsilon} = \frac{1}{2} [\nabla \mathbf{v}^s + (\nabla \mathbf{v}^s)^T], \quad (3)$$

with the superscript ‘ $T$ ’ denoting the transpose operation.

In fluid regions, the wavefield is described by coupled partial differential equations that represent the conservation of linear momentum,

$$\rho^f \dot{\mathbf{v}}^f + \nabla p = 0, \quad (4)$$

and the conservation of mass,

$$\dot{p} + \rho^f (c^f)^2 \nabla \cdot \mathbf{v}^f = s^f, \quad (5)$$

where  $p$  is the pressure,  $\rho^f$  is the fluid density,  $c^f$  is the P-wave velocity,  $\mathbf{v}^f$  is the particle velocity and  $s^f$  describes the pressure source; the superscript ‘ $f$ ’ indicates a material property or wavefield variable defined in the fluid medium.

## Boundary conditions

The boundary conditions coupling acoustic and elastic media are the continuity of traction and of the normal component of the particle velocity, known as the dynamic and kinematic boundary conditions, respectively (Sethi et al., 2021, 2022). The continuity of traction is given by:

$$\boldsymbol{\sigma} \cdot \mathbf{n} = -p \mathbf{n}, \quad (6)$$

where  $p$  is pressure and  $\mathbf{n}$  is the unit vector normal to the fluid/solid interface. The continuity of the normal component of the particle velocity is expressed as

$$\mathbf{v}^f \cdot \mathbf{n} = \mathbf{v}^s \cdot \mathbf{n}. \quad (7)$$

The boundary condition at the top of the acoustic layer (i.e., at the water–air interface) requires setting the pressure to zero:

$$p = 0. \quad (8)$$

## Coupled fluid/solid inverse problem

Elastic full-waveform inversion for ocean-bottom data can be formulated as the minimization of the following objective function (Menke, 2018):

$$\min_{\mathbf{m}} \chi(\mathbf{m}) = \frac{1}{2} \sum_{s,r} \|\mathbf{W}(\mathbf{d}_{\text{obs}} - \mathbf{d}_{\text{cal}})\|^2, \quad (9)$$

where  $\mathbf{m}$  represents the model parameters for elastic VTI media,  $\mathbf{d} = [p, v_x^s, v_z^s]$ ,  $\mathbf{d}_{\text{obs}}$  denotes the recorded data,  $\mathbf{d}_{\text{cal}}$  is the data calculated for a certain trial model,  $\mathbf{W}$  is the data covariance matrix (or the weighting matrix) and  $\|\cdot\|^2$  indicates the  $L_2$ -norm. We use the following weighting matrix (Vigh et al., 2014) for all our numerical experiments:

$$\mathbf{W} = \begin{pmatrix} \mathbf{I}_p & 0 \\ 0 & \rho^r V_{P0}^r \mathbf{I}_v \end{pmatrix}, \quad (10)$$

where  $\mathbf{I}_p$  is the  $1 \times 1$  identity matrix,  $\mathbf{I}_v$  is the  $2 \times 2$  identity matrix and  $\rho^r$  and  $V_{P0}^r$  are the density and P-wave vertical velocity at the receiver locations, respectively. Note that after the application of the weighting matrix, the particle-velocity components have the same units and similar amplitudes. The model parameters are updated via an efficient local gradient-based approach:

$$\mathbf{m}_{i+1} = \mathbf{m}_i + \mu \mathbf{h}_i, \quad (11)$$

where  $\mathbf{m}_i$  is the model-parameter vector at the  $i$ th iteration,  $\mathbf{h}_i$  defines the descent direction and  $\mu$  is the step length. The gradients of the objective function can be computed via the adjoint-state method (Sethi, 2023):

$$\frac{\partial \chi(\mathbf{m})}{\partial \mathbf{m}} = \sum_{ijkl} \frac{\partial \chi}{\partial c_{ijkl}} \frac{\partial c_{ijkl}}{\partial \mathbf{m}}. \quad (12)$$

The gradients are obtained from a pressure-displacement formulation of a fluid/solid coupled system, where the solid has the VTI symmetry. The exact full-waveform inversion gradients and the relationships between the stiffness coefficients and VTI parameters can be found in Sethi (2023). For computing the gradient with respect to density, we use the following expression (Sethi, 2023):

$$\frac{\partial \chi(\mathbf{m})}{\partial \rho} = \int_0^T \mathbf{v}_i \mathbf{v}_i^* dt, \quad (13)$$

where  $\mathbf{v}_i$  and  $\mathbf{v}_i^*$  are the forward and adjoint velocity wavefields, respectively.

## NUMERICAL EXAMPLES

Here, we test our coupled fluid/solid mimetic-finite-difference-based elastic full-waveform inversion (EFWI) algorithm for hard and soft water bottoms. A multiscale approach to parameter updating is employed by starting from lower frequency bands towards higher frequencies (Bunks et al., 1995). We use a velocity-based parameterization for (VTI) media (Kamath & Tsvankin, 2016) that includes the vertical P- and S-wave velocities ( $V_{P0}$  and  $V_{S0}$ ), and the

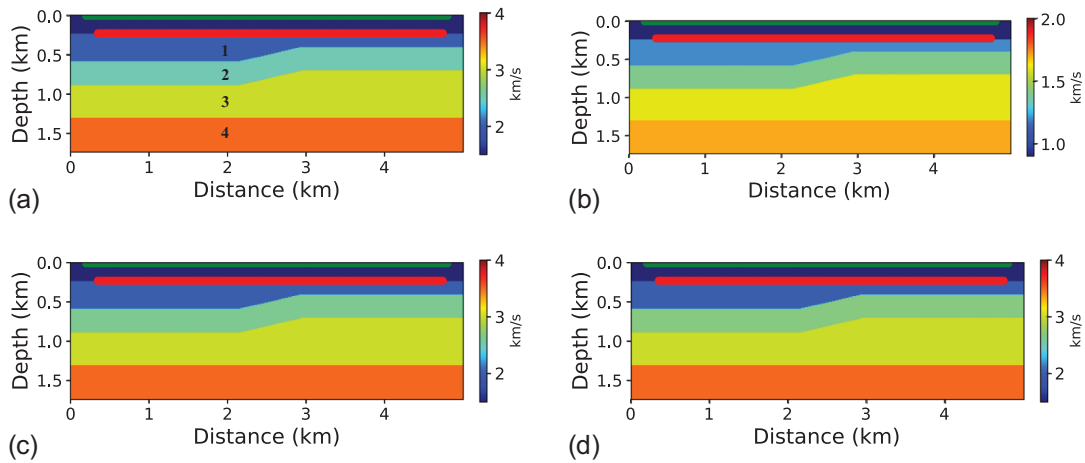


**FIGURE 1** High-velocity (hard) water bottom model. (a) The P-wave vertical velocity ( $V_{P0}$ ), (b) the S-wave vertical velocity ( $V_{S0}$ ), (c) the P-wave normal-moveout velocity ( $V_{\text{nm},P}$ ), and (d) the P-wave horizontal velocity ( $V_{\text{hor},P}$ ). The sources and receivers are marked by green and red dots, respectively. The Thomsen anisotropy parameters in layers 2 and 3 are ( $\delta = 0.1$ ,  $\epsilon = 0.15$ ) and ( $\delta = 0.12$ ,  $\epsilon = 0.2$ ), respectively.

P-wave normal-moveout and horizontal velocities ( $V_{\text{nm},P}$  and  $V_{\text{hor},P}$ ):  $V_{\text{nm},P} = V_{P0} \sqrt{1 + 2\delta}$ ;  $V_{\text{hor},P} = V_{P0} \sqrt{1 + 2\epsilon}$ , where  $\epsilon$  and  $\delta$  are Thomsen parameters (Thomsen, 1986; Tsvankin, 2012). The parameters  $V_{P0}$ ,  $V_{S0}$ ,  $V_{\text{nm},P}$ , and  $V_{\text{hor},P}$  control P- and SV-wave propagation in VTI models. The density is assumed to be known in all tests, except for one example discussed below.

## Hard water bottom

First, we consider a two-dimensional layered model with a hard water bottom ( $V_{P0} \approx 1800$  m/s) in Figure 1. The wavefield is excited by 116 point explosive sources placed at 10-m depth with a 40-m interval. The source signal is the Ricker wavelet with a 10-Hz peak frequency. The pressure and both particle-velocity components are recorded by 440 receivers placed on the seafloor. The multiscale FWI algorithm operates with four frequency bands (0–2, 0–5, 0–10, 0–20 Hz). The source wavelet and receiver data are first filtered in the 0–2 Hz frequency range. The inversion algorithm moves to the next frequency stage (0–5 Hz) once the objective function reaches a certain tolerance level, and so on.

A one-dimensional medium with constant vertical velocity gradients is used as the initial model for EFWI (Figure 2). The VTI parameters inverted from the pressure data are sufficiently accurate in the shallow part of the model (Figure 3). However, the estimates of  $V_{S0}$ ,  $V_{\text{hor},P}$ , and  $V_{\text{nm},P}$  degrade with increasing depth due to the lack of shear-wave information in pressure records and parameter trade-offs ( $V_{P0}$  remains well-constrained). Figure 4 shows the inversion results obtained from the vertical particle-velocity component ( $v_z$ ). There is a clear improvement in  $V_{S0}$ , especially in layer 3 (Figure 4a) and in  $V_{\text{nm},P}$  at the boundary between layers 3

and 4 (Figure 4c). Figure 5 shows the EFWI output obtained by simultaneously inverting both the vertical and horizontal particle-velocity components. There are improvements in the velocity  $V_{S0}$  (Figure 5b) compared to the EFWI of hydrophone data (Figure 3). However, the inversion results using the vertical component alone are generally superior (Figure 4).

Next, we perform the inversion of the multicomponent data using a two-stage (sequential) strategy. First, a multiscale approach is used to estimate the VTI parameters from the vertical component. These results (Figure 4) serve as the initial model for inverting the horizontal particle velocity. However, the improvements achieved by adding the horizontal component are marginal.

The material property estimates obtained using the weighted objective function in Equation (9) (i.e., by inverting all data components simultaneously) are shown in Figure 6. The accuracy of parameter estimation is comparable to that in Figure 5 but lower than that for the component  $v_z$  alone (Figure 4). We also test a three-stage sequential strategy using all data components. First, the hydrophone records alone are inverted for the model parameters. Then the obtained results are used to build the initial model for the next stage inversion of  $v_z$ . Finally, at the last stage, we invert the horizontal particle velocity. This sequential approach performs well, especially for estimating  $V_{S0}$  and  $V_{\text{nm},P}$  in layers 3 and 4 (see Figure 7). Figure 8 shows the vertical parameter profiles at  $x = 2$  km, which confirm that the sequential strategy provides the best inversion results.

## Soft water bottom

Next, we consider a model with a soft water bottom (see Figure 9). The model is similar to that in the previous example

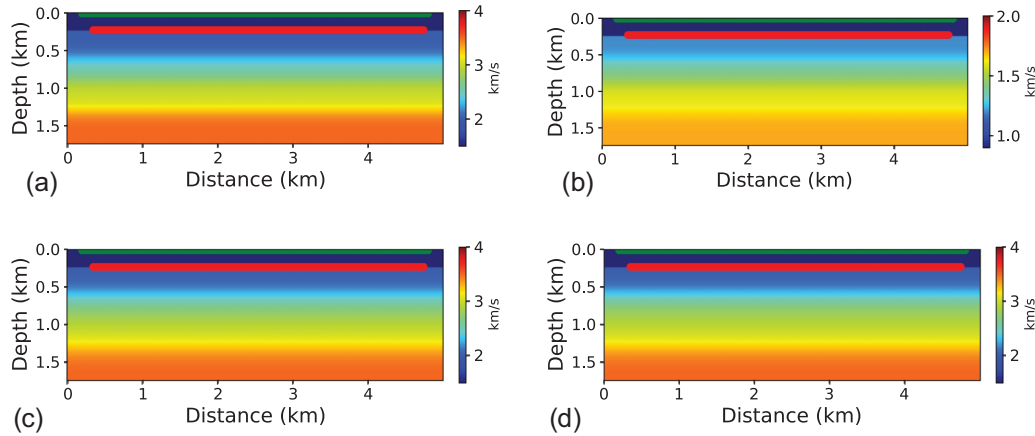


**FIGURE 2** Initial models for EFWI: (a)  $V_{P0}$ , (b)  $V_{S0}$ , (c)  $V_{nmo,P}$ , and (d)  $V_{hor,P}$ .

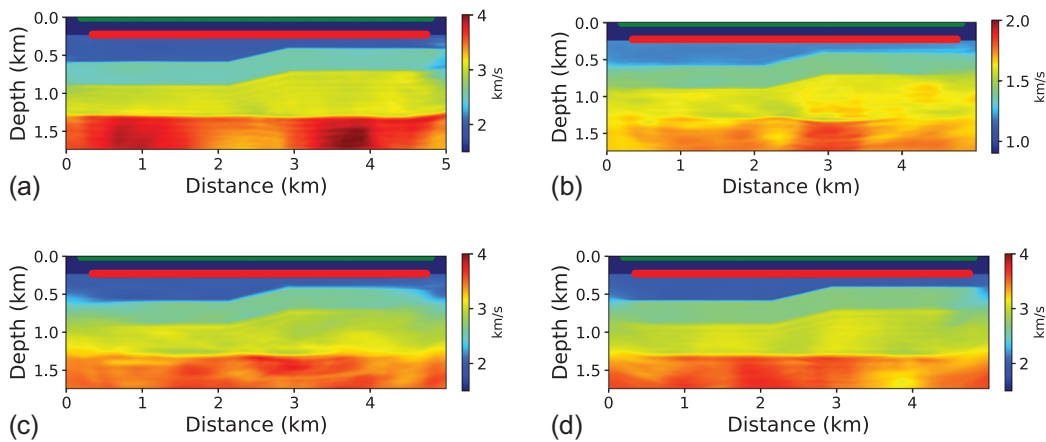


**FIGURE 3** Inversion results for the model in Figure 1 obtained from hydrophone data: (a)  $V_{P0}$ , (b)  $V_{S0}$ , (c)  $V_{nmo,P}$ , and (d)  $V_{hor,P}$ .

but the velocities  $V_{P0}$  and  $V_{S0}$  in the underwater layer are much smaller. Also, the velocities  $V_{hor,P}$  and  $V_{nmo,P}$  in layer 4 are lower than in layer 3 (Figure 9c,d). The acquisition geometry is kept the same as in the previous test. Figure 10 shows the pressure and particle-velocity components for the source placed at  $[x, z] = [1.25, 0.005]$  km. The water-bottom multiples are much weaker compared to the hard-water-bottom case. The mode-converted (PSP) waves are clearly visible in pressure records because of their large reflection moveouts (i.e., low moveout velocities).

The inversion of the hydrophone data using a one-dimensional initial model with constant vertical gradients yields the parameters in Figure 11. The clear kinematic separation of reflections from the deeper layers improves the overall estimation of the medium parameters. Similar inversion results are obtained using the vertical particle-velocity component. For this model, incorporating the sequential strategy described above that involves the pressure and both particle velocities yields only minor improvements in parameter estimation.

## VTI Marmousi model

Finally, we test our algorithm on the VTI Marmousi model, which is highly heterogeneous (Figure 12). The initial model in Figure 13 is obtained by applying strong Gaussian smoothing (the standard deviation of the Gaussian kernel is set to 20, and smoothing is repeated five times). We use a multiscale approach with four frequency bands (2–3, 2–5, 2–10, 2–20 Hz); frequencies below 2 Hz are removed to make the test more realistic. The wavefield is excited by 110 sources placed at 10 m depth with a 30-m interval. The source signal is a Ricker wavelet with a 10-Hz peak frequency. A total of 330 receivers that record both the pressure and particle-velocity components are placed on the seafloor with a 10-m interval.

Figure 14 shows the parameters inverted from the hydrophone data. The long-wavelength features of all parameters are recovered with sufficient accuracy. However, there are issues in resolving the velocity  $V_{S0}$ , and some shorter-wavelength features in  $V_{hor,P}$  and  $V_{nmo,P}$  are missing. The

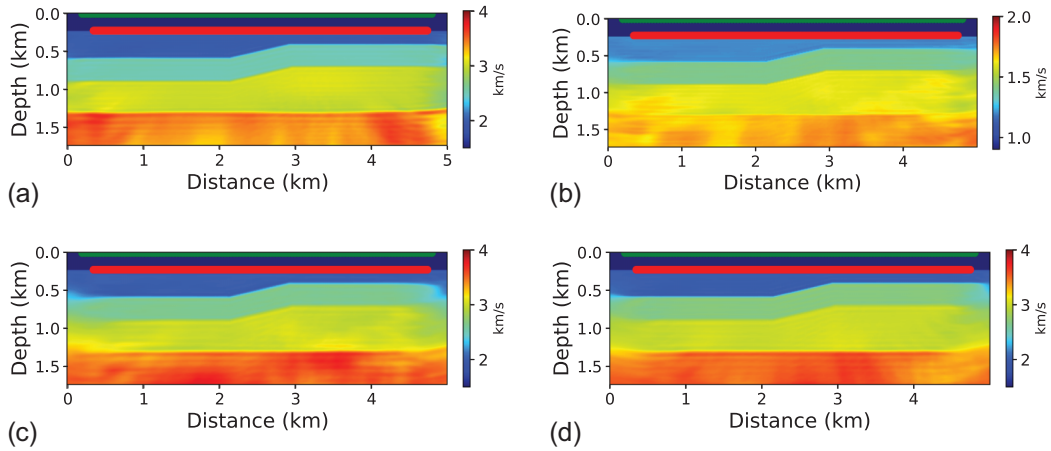


**FIGURE 4** Inversion results for the model in Figure 1 obtained from the vertical particle velocity ( $v_z$ ): (a)  $V_{P0}$ , (b)  $V_{S0}$ , (c)  $V_{nmo, P}$ , and (d)  $V_{hor, P}$ .

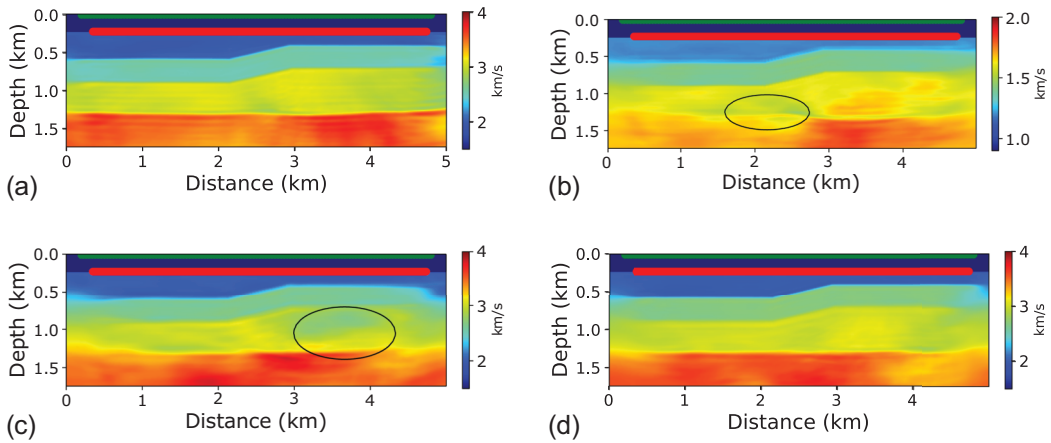


**FIGURE 5** Inversion results for the model in Figure 1 obtained by using both particle-velocity components simultaneously: (a)  $V_{P0}$ , (b)  $V_{S0}$ , (c)  $V_{nmo, P}$ , and (d)  $V_{hor, P}$ . The black circles mark the areas where there is a major degradation in parameter estimates compared to the results in Figure 4.

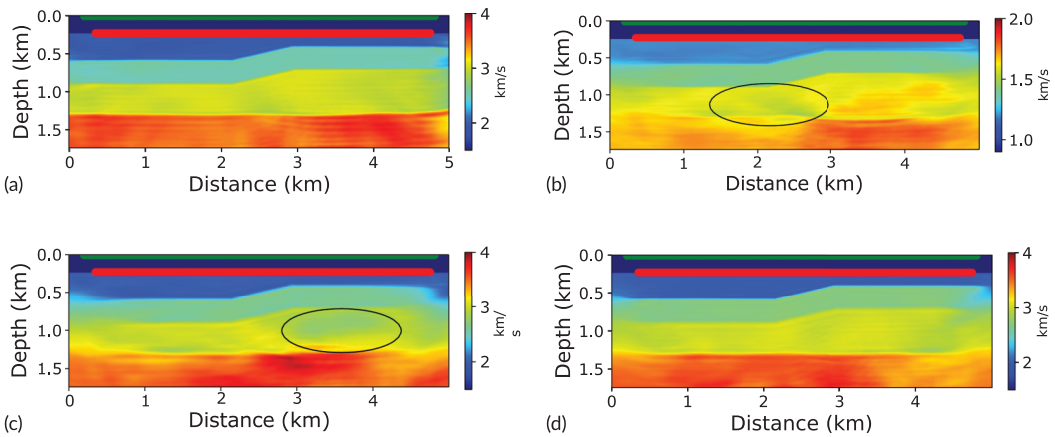


**FIGURE 6** Results of inverting all data components (pressure and both particle velocities) simultaneously (see Equation 9) for the model in Figure 1: (a)  $V_{P0}$ , (b)  $V_{S0}$ , (c)  $V_{nmo, P}$ , and (d)  $V_{hor, P}$ . The black ellipses mark the areas where there is a major degradation in parameter estimates compared to the results in Figure 4.

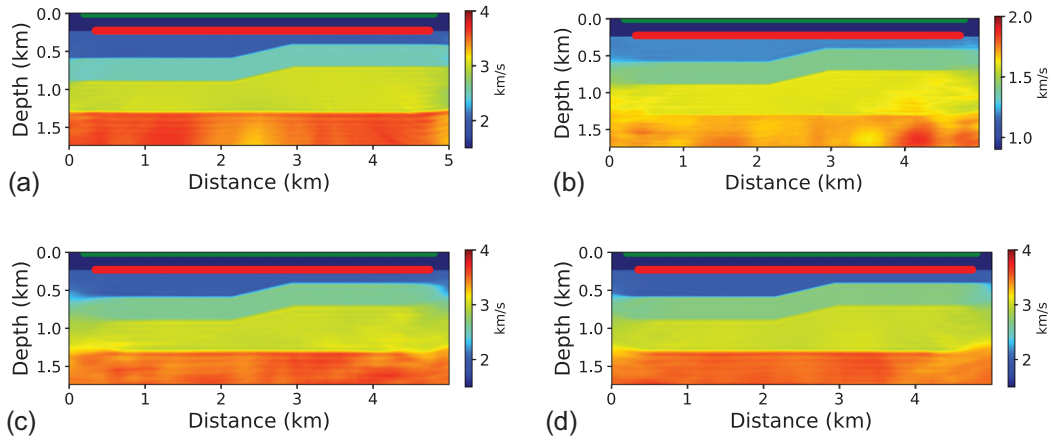


**FIGURE 7** Results of inverting all data components (pressure and both particle velocities) using the sequential strategy for the model in Figure 1: (a)  $V_{p0}$ , (b)  $V_{S0}$ , (c)  $V_{nmo, P}$ , and (d)  $V_{hor, P}$ .

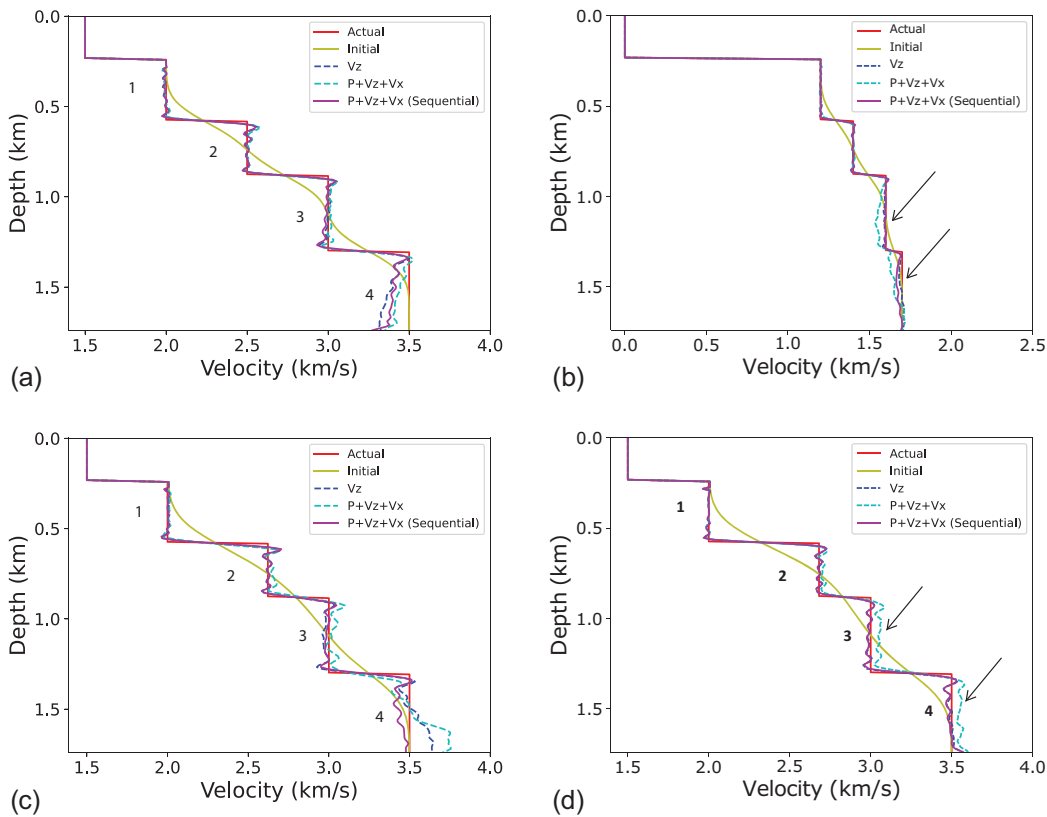


**FIGURE 8** Vertical parameter profiles at  $x = 2$  km: (a)  $V_{p0}$ , (b)  $V_{S0}$ , (c)  $V_{nmo, P}$ , and (d)  $V_{hor, P}$ . The arrows mark the improvements achieved by the sequential inversion strategy. The numbers correspond to the layers marked in Figure 1a.

inversion of the vertical particle-velocity component produces much better results for all VTI parameters (Figure 15). Using the combined objective function that includes either all three types of data or the two particle-velocity components does not improve the inversion results and even leads to their minor degradation.

Next, we test a sequential strategy that involves just the particle velocities. The vertical particle velocity is inverted

first via a multiscale approach. Then we apply FWI to the horizontal particle velocity with the initial model built using the first-stage results. Including the horizontal component improves parameter estimation, especially the velocities  $V_{S0}$  and  $V_{nmo, P}$  (see Figure 16). For the sequential strategy involving all data components (see above), we first invert the hydrophone records followed by the inversion of the vertical and horizontal particle velocities. The results show

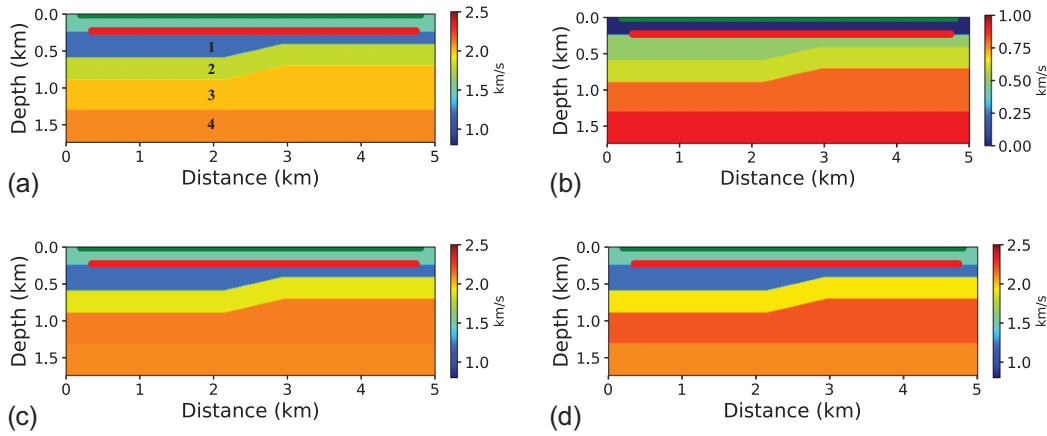


**FIGURE 9** Model with a low-velocity (soft) water bottom: (a)  $V_{p0}$ , (b)  $V_{S0}$ , (c)  $V_{nmo, P}$ , and (d)  $V_{hor, P}$ . The Thomsen parameters in layers 2 and 3 are the same as for the model in Figure 1.

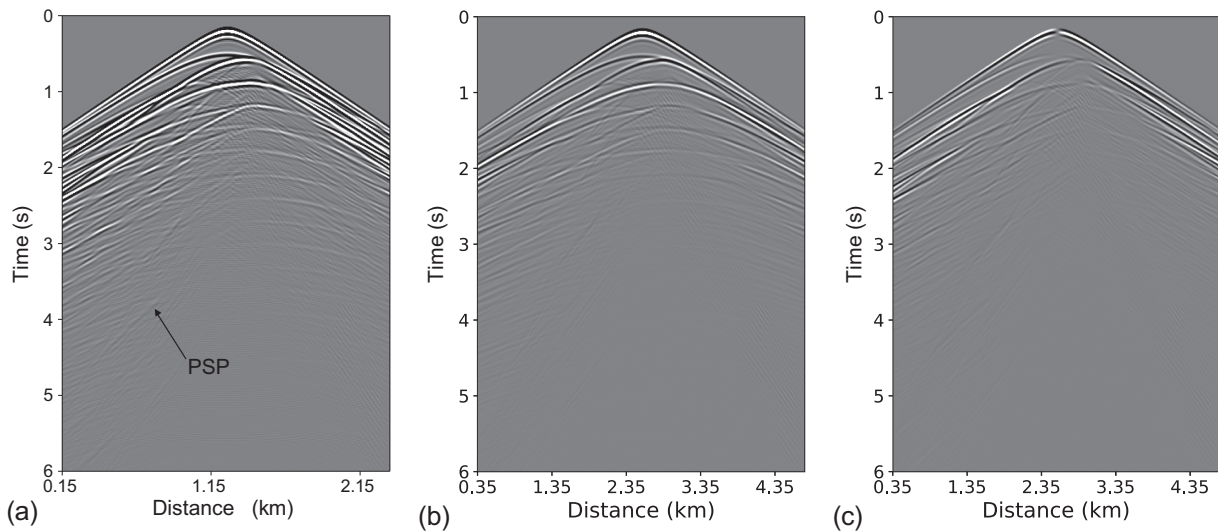


**FIGURE 10** Seismograms for the model in Figure 9. The source is placed at  $[x, z] = [1.25, 0.005]$  km. (a) The hydrophone (pressure) record, (b)  $V_Z$  and (c)  $V_X$ .

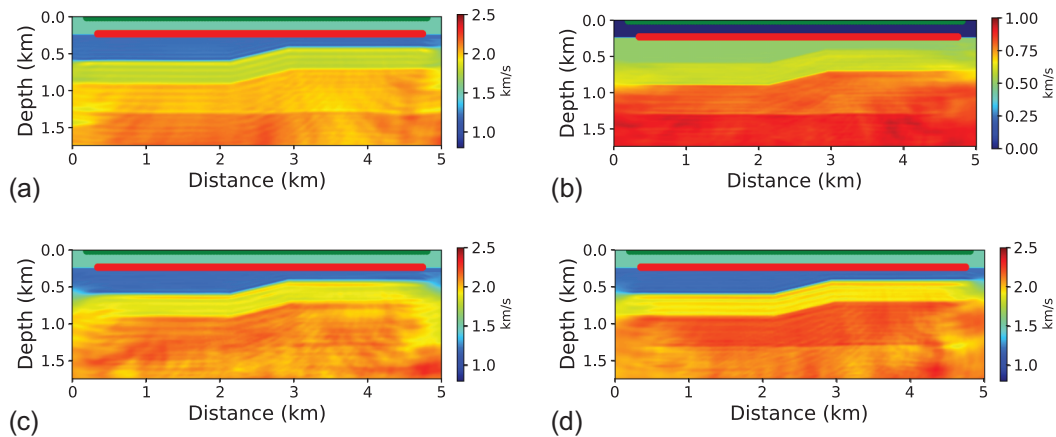


**FIGURE 11** Inverted model for the low-velocity (soft) water bottom obtained from the hydrophone data: (a)  $V_{p0}$ , (b)  $V_{S0}$ , (c)  $V_{nmo, P}$ , and (d)  $V_{hor, P}$ .



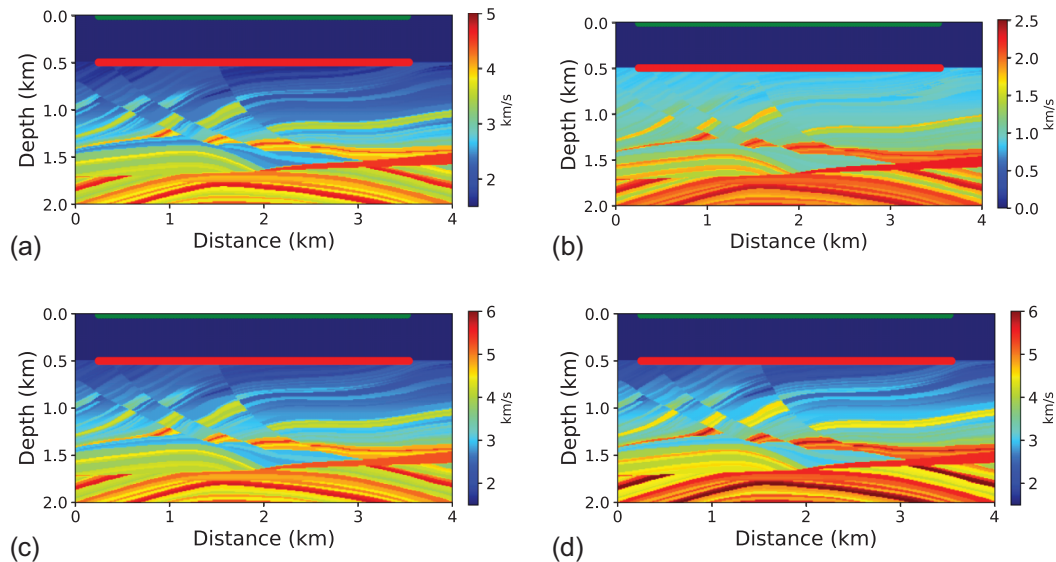


**FIGURE 12** Parameters of the VTI Marmousi model: (a)  $V_{p0}$ , (b)  $V_{S0}$ , (c)  $V_{nmo,P}$ , and (d)  $V_{hor,P}$ .

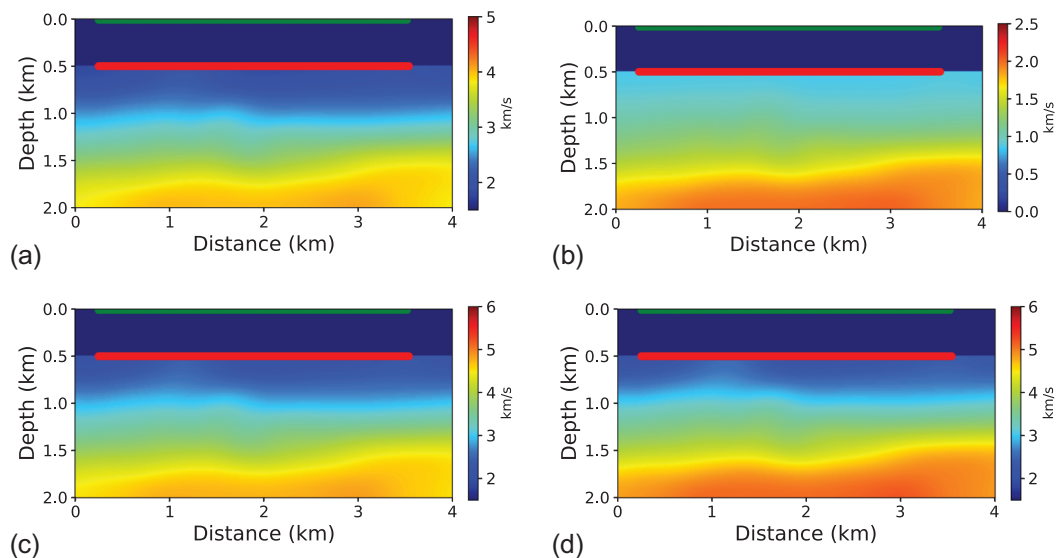


**FIGURE 13** Initial models obtained by Gaussian smoothing of the actual model parameters in Figure 12: (a)  $V_{p0}$ , (b)  $V_{S0}$ , (c)  $V_{nmo,P}$ , and (d)  $V_{hor,P}$ .

minor improvements in comparison to the sequential strategy involving just the particle-velocity components.

To test the robustness of the sequential strategy that operates with all data components, we contaminate the data with pseudo-random Gaussian noise (the signal-to-noise ratio = 15). The inverted model (Figure 17) is satisfactory, but the noise causes some deterioration in the resolution and accuracy of the estimated velocities.

## Density inversion

We also extended our algorithm to invert for the density in addition to the velocity parameters. Figure 18 shows the inver-

sion results for the VTI Marmousi model obtained using a sequential strategy that involves all three data components including the pressure and both particle velocities. We used the same initial models for the velocities as those in Figure 13. The initial density model (Figure 18e) is obtained by Gaussian smoothing of the actual density field with the same smoothing parameters as those for the velocity models. The acquisition parameters and the frequency bands for the multiscale approach are kept the same as in the previous experiments.

There is some degradation in the estimated velocity models compared to the previous tests, in part due to the tradeoffs between the velocities and density. However, our algorithm is able to recover the overall structure for all parameters including density (Figure 18). The inversion results when using

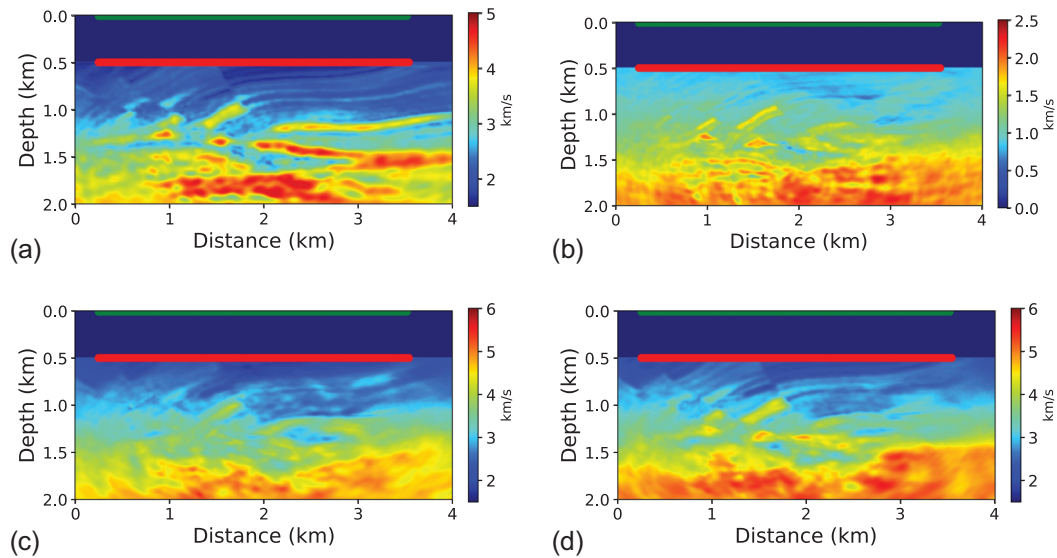


**FIGURE 14** Parameters of the Marmousi model inverted from the hydrophone data: (a)  $V_{P0}$ , (b)  $V_{S0}$ , (c)  $V_{nmo,P}$ , and (d)  $V_{hor,P}$ .

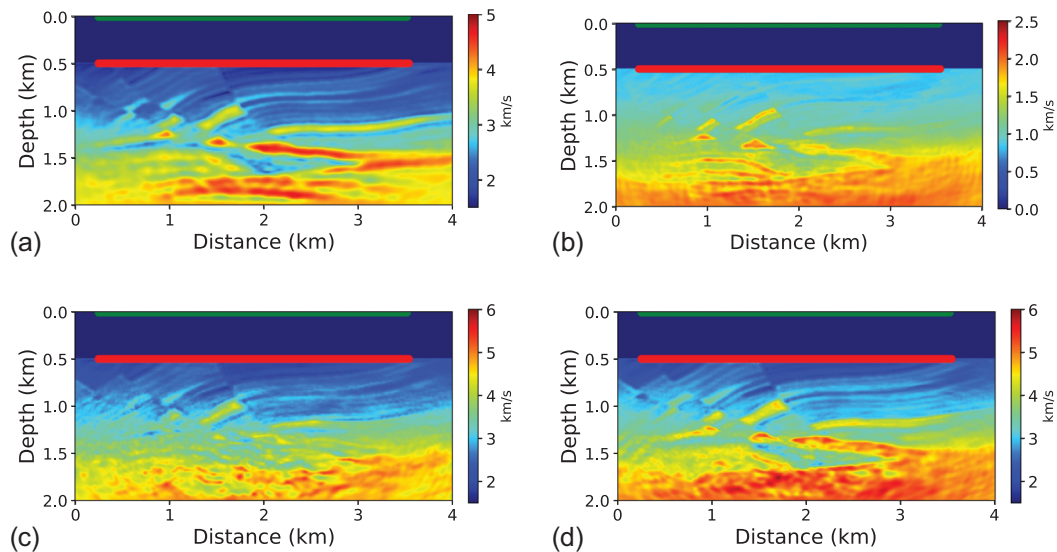


**FIGURE 15** Parameters of the Marmousi model inverted from the vertical particle velocity: (a)  $V_{P0}$ , (b)  $V_{S0}$ , (c)  $V_{nmo,P}$ , and (d)  $V_{hor,P}$ .

only the hydrophone data were suboptimal, especially for density. Inverting the vertical particle-velocity component gives results similar to those in Figure 18.

## DISCUSSION

The proposed sequential strategy involving all data components (pressure and both particle velocities) performs well for different types of the water bottom. However, pressure data alone can be used to recover the VTI parameters with sufficient accuracy if long-offset (with respect to the target depth) data are available. Inversion of the vertical particle velocity gives results similar to those for the pressure data. Including

the horizontal particle-velocity component in the later stages of the sequential inversion leads to an overall improvement in parameter estimation.

For the VTI Marmousi model, it is difficult to recover short-wavelength features of the velocities  $V_{nmo,P}$  and  $V_{hor,P}$  from the pressure data alone because the offset/depth ratio for the deeper part of the model is less than two. The sensitivity analysis by Kamath and Tsvankin (2016) for the velocity-based VTI parameterization indicates that estimation of  $V_{nmo,P}$  and  $V_{hor,P}$  from P-wave data requires incidence angles exceeding  $40^\circ$ . Including multicomponent data is highly beneficial for resolving the density and those small-scale features in  $V_{nmo,P}$  and  $V_{hor,P}$ . Among the tested strategies, inverting all data components sequentially starting with hydrophone records

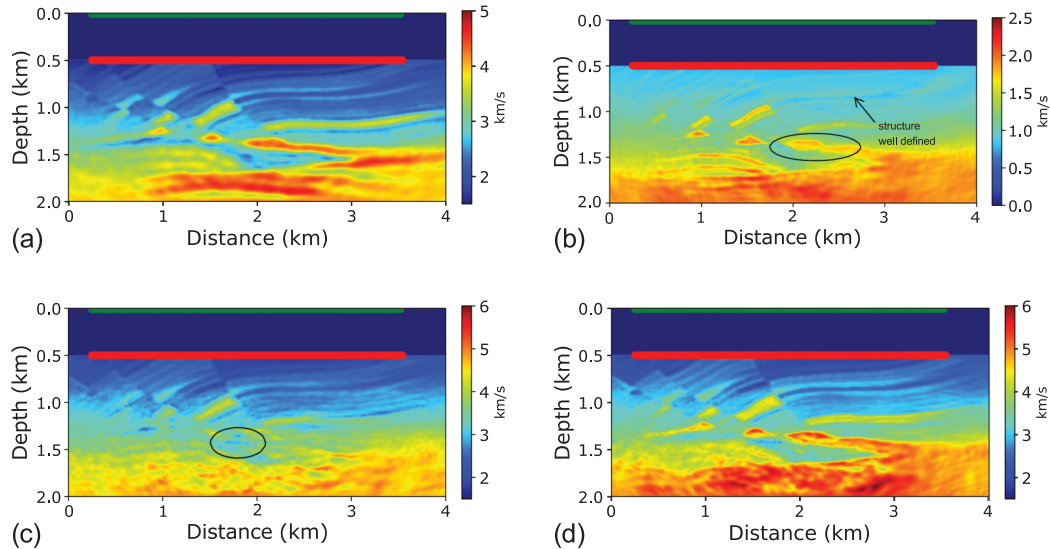


**FIGURE 16** Parameters of the Marmousi model inverted from the particle-velocity components using the sequential strategy: (a)  $V_{p0}$ , (b)  $V_{S0}$ , (c)  $V_{nmo, P}$ , and (d)  $V_{hor, P}$ . The black ellipses mark the improvements achieved by including the horizontal component.

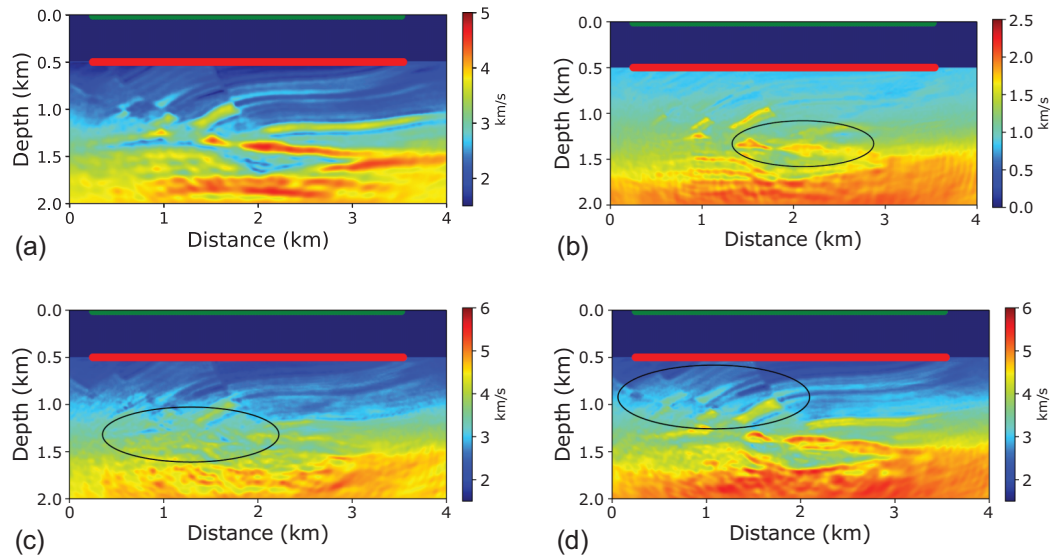


**FIGURE 17** Parameters of the Marmousi model inverted from all data components using the sequential strategy. The the input data are contaminated with Gaussian noise that has a signal-to-noise ratio equal to 15. The estimated (a)  $V_{p0}$ , (b)  $V_{S0}$ , (c)  $V_{nmo, P}$ , and (d)  $V_{hor, P}$ . The black ovals indicate the degradation of results in comparison to those in Figure 16.

typically gives the best results. The simultaneous inversion of all data components proves to be generally unsuccessful, likely due to a more complicated topology of the objective function, which agrees with the results of Kamath and Tsvankin (2016).

## CONCLUSIONS

We presented an efficient framework for elastic full-waveform inversion of multicomponent data based on a coupled

fluid/solid finite-difference modelling algorithm. The developed methodology is applied to VTI media but it is straightforward to extend it to models with lower symmetry, such as tilted orthorhombic, using the results of Sethi et al. (2022). The adjoint-state method was employed to obtain the adjoint of the coupled fluid/solid system and derive the gradients of the objective function. We tested several multiscale FWI strategies for two-dimensional VTI media that operate with hydrophone records and vertical and horizontal particle velocities. A sequential approach based on inverting a single data component at a time (starting from hydrophone records)

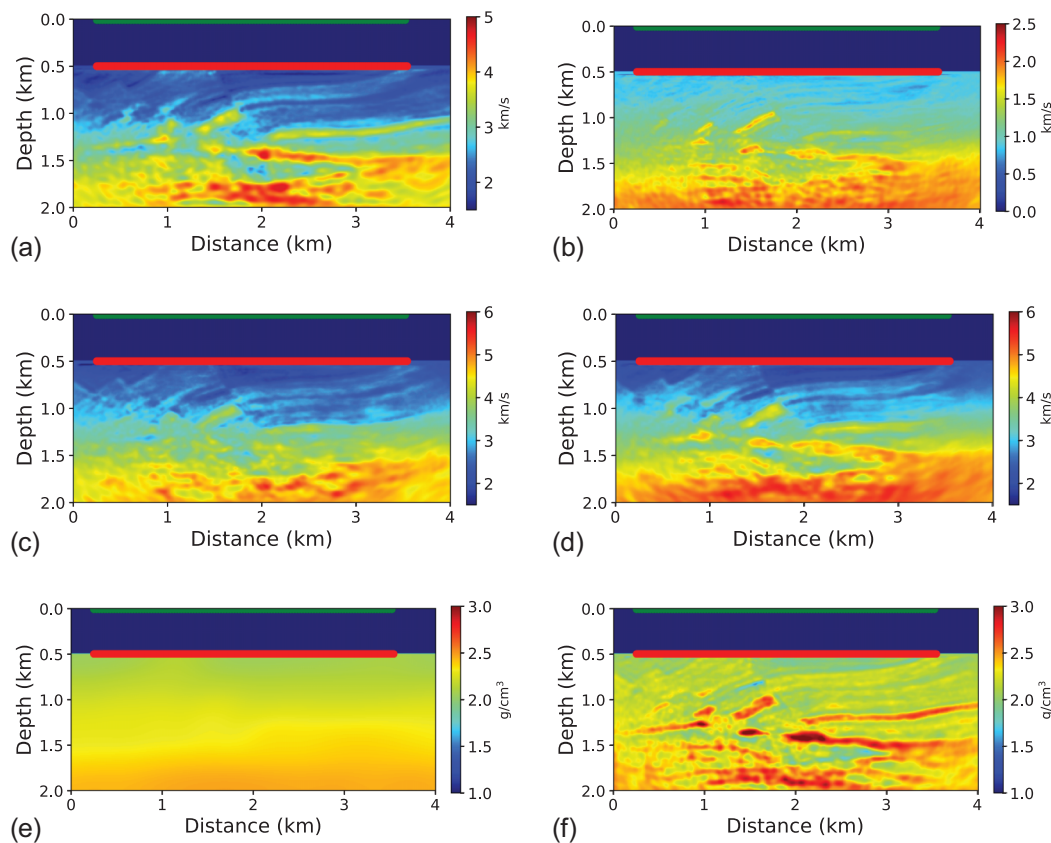


**FIGURE 18** Parameters of the Marmousi model including density obtained from all data components using the sequential strategy: (a)  $V_{p0}$ , (b)  $V_{S0}$ , (c)  $V_{nmo,P}$ , (d)  $V_{hor,P}$ , (e)  $\rho$  (initial), and (f)  $\rho$  (inverted).

generally gives the best results for both hard and soft water bottom. Pressure (hydrophone) data alone may be sufficient for estimating the VTI parameters with acceptable accuracy if long-offset data (with the offset-to-depth ratio approaching three) are available. Adding the horizontal particle-velocity component in the later stages of inversion improves the estimation of the velocities  $V_{S0}$  and  $V_{hor,P}$ . The sequential strategy is also capable of reconstructing density, although inverting for density somewhat reduces the accuracy of the estimated velocity parameters.


#### ACKNOWLEDGEMENTS

We thank the sponsors of the Consortium Project on Seismic Inverse Methods for Complex Structures at the Center for Wave Phenomena (CWP), Colorado School of Mines, whose support made this research possible. We are grateful to Sagar Singh (Nvidia Corporation, formerly CWP) for many useful discussions. We thank Alexey Stovas and two anonymous reviewers for helpful comments that improved the quality of the manuscript. We also acknowledge the Mines HPC facility for computing time allocations on the *Wendian* cluster.

#### DATA AVAILABILITY STATEMENT

The data that support the findings of this study are available from the corresponding author upon request.

#### ORCID

Harpreet Sethi  <https://orcid.org/0000-0001-5644-5701>

#### REFERENCES

- Bunks, C., Saleck, F.M., Zaleski, S. & Chavent, G. (1995) Multiscale seismic waveform inversion. *Geophysics*, 60(5), 1457–1473.
- Cao, J., Brossier, R., Górszczyk, A., Métivier, L. & Virieux, J. (2022) 3-D multiparameter full-waveform inversion for ocean-bottom seismic data using an efficient fluid-solid coupled spectral-element solver. *Geophysical Journal International*, 229(1), 671–703.
- Chen, G., Yang, W., Liu, Y., Wang, H. & Huang, X. (2022) Salt structure elastic full waveform inversion based on the multiscale signed envelope. *IEEE Transactions on Geoscience and Remote Sensing*, 60, 1–12.
- Farfour, M. & Yoon, W.J. (2016) A review on multicomponent seismology: a potential seismic application for reservoir characterization. *Journal of Advanced Research*, 7(3), 515–524.
- Gholami, Y., Brossier, R., Operto, S., Ribodetti, A. & Virieux, J. (2013) Which parameterization is suitable for acoustic vertical transverse isotropic full waveform inversion? Part 1: Sensitivity and trade-off analysis. *Geophysics*, 78(2), R81–R105.
- Guittou, A. & Alkhalifah, T. (2017) A parameterization study for elastic vti full-waveform inversion of hydrophone components: synthetic and North Sea field data examples. *Geophysics*, 82(6), R299–R308.
- Irnaka, T.M., Brossier, R., Métivier, L., Bohlen, T. & Pan, Y. (2022) 3-D multicomponent full waveform inversion for shallow-seismic target:



- Ettlingen line case study. *Geophysical Journal International*, 229(2), 1017–1040.
- Kamath, N. & Tsvankin, I. (2016) Elastic full-waveform inversion for VTI media: Methodology and sensitivity analysis. *Geophysics*, 81(2), C53–C68.
- Kamath, N., Tsvankin, I. & Díaz, E. (2017) Elastic full-waveform inversion for VTI media: A synthetic parameterization study. *Geophysics*, 82(5), C163–C174.
- Menke, W. (2018) *Geophysical data analysis: Discrete inverse theory*. Academic press.
- Mora, P. (1987) Nonlinear two-dimensional elastic inversion of multioffset seismic data. *Geophysics*, 52(9), 1211–1228.
- Operto, S., Miniussi, A., Brossier, R., Combe, L., Métivier, L., Monteiller, V., Ribodetti, A. & Virieux, J. (2015) Efficient 3-D frequency-domain mono-parameter full-waveform inversion of ocean-bottom cable data: application to Valhall in the visco-acoustic vertical transverse isotropic approximation. *Geophysical Journal International*, 202(2), 1362–1391.
- Pladys, A., Brossier, R., Kamath, N. & Métivier, L. (2022) Robust full-waveform inversion with graph-space optimal transport: application to 3D ocean-bottom cable Valhall data. *Geophysics*, 87(3), R261–R280.
- Plessix, R.E. & Cao, Q. (2011) A parametrization study for surface seismic full waveform inversion in an acoustic vertical transversely isotropic medium. *Geophysical Journal International*, 185(1), 539–556.
- Qu, Y., Guan, Z., Li, J. & Li, Z. (2020) Fluid-solid coupled full-waveform inversion in the curvilinear coordinates for ocean-bottom cable data. *Geophysics*, 85(3), R113–R133.
- Sears, T.J., Singh, S. & Barton, P. (2008) Elastic full waveform inversion of multi-component OBC seismic data. *Geophysical Prospecting*, 56(6), 843–862.
- Sethi, H. (2023) Efficient modeling and waveform inversion of multi-component seismic data for anisotropic media. PhD thesis, Colorado School of Mines.
- Sethi, H., Shragge, J. & Tsvankin, I. (2021) Mimetic finite-difference coupled-domain solver for anisotropic media. *Geophysics*, 86, T45–T59.
- Sethi, H., Shragge, J. & Tsvankin, I. (2022) Tensorial elastodynamics for coupled acoustic/elastic anisotropic media: incorporating bathymetry. *Geophysical Journal International*, 228(2), 999–1014.
- Sun, M. & Jin, S. (2020) Multiparameter elastic full waveform inversion of ocean bottom seismic four-component data based on a modified acoustic-elastic coupled equation. *Remote Sensing*, 12(17), 2816.
- Tarantola, A. (1986) A strategy for nonlinear elastic inversion of seismic reflection data. *Geophysics*, 51(10), 1893–1903.
- Thomsen, L. (1986) Weak elastic anisotropy. *Geophysics*, 51(10), 1954–1966.
- Tsvankin, I. (2012) *Seismic signatures and analysis of reflection data in anisotropic media* (3rd ed.). Houston, TX: Society of Exploration Geophysicists.
- Vigh, D., Jiao, K., Watts, D. & Sun, D. (2014) Elastic full-waveform inversion application using multicomponent measurements of seismic data collection. *Geophysics*, 79(2), R63–R77.
- Zelt, C. & Smith, R. (1992) Seismic traveltime inversion for 2-D crustal velocity structure. *Geophysical Journal International*, 108(1), 16–34.

**How to cite this article:** Sethi, H., Tsvankin, I. & Shragge, J. (2024) Methodology of elastic full-waveform inversion of multicomponent ocean-bottom data for anisotropic media. *Geophysical Prospecting*, 72, 604–616.  
<https://doi.org/10.1111/1365-2478.13440>